An Enhanced Electro-Optic Chaos Secure Communication System Immune to Time Delay Signature Extraction

Huaxi Huang, Zhenhua Li, Xiaojing Gao, and Mengfan Cheng, *Senior Member, IEEE*

***Abstract*—Time delay signature (TDS) is a key issue that affects the security performance of optical chaos communication. Currently, the autocorrelation function (ACF) and delayed mutual information (DMI) are two crucial methods to extract the TDS. Several strategies have been proposed to resist statistical analysis (i.e., ACF and DMI). However, a dynamic inverse modeling method has been proposed to identify TDS by utilizing the strong nonlinear inversion capability of deep learning, which brings about new threat. To resist this analysis, we propose a stratagem that one can increase the nonlinear dimensionality of the chaos system at the transmitter and concurrently reduce the dimensionality of transmitted signals, leading to "deficiency of data dimensionality". A three-dimensional chaotic system is designed as the transmitter and only one-dimensional signal is transmitted for communication. Furthermore, a hybrid receiver is designed. The nonlinear model of the response system is realized by cooperation of an analog electro-optical link and a neural network in digital domain. The architecture not only destroys the possibility of TDS extraction but also preserves all necessary information required for chaos synchronization with low-complexity implementation.**

***Index Terms*—Physical layer security, time delay concealment, deep learning.**

I. Introduction

In THE field of optical secure communication [1]–[3], time delayed optical chaos system has been highlighted due to its superior advantages of wide-frequency spectrum and high dynamical complexity [4]–[6]. Particularly, because of good stability, low cost, and large Lyapunov dimension even if only a few physical degrees of freedom are involved, time delayed electro-optic (EO) chaos system has been widely investigated and become one of the most feasible optical chaos sources [7]–[9]. In these systems, time delay plays an essential role in generating the chaos carrier and it is used as the ideal key to enhance the security. Suppression of the TDS significantly influences the degree of security [10]–[12]. Generally, an eavesdropper can reconstruct the chaotic system to break the security once the TDS is determined. However, it is confirmed that several methods can be used to recover the TDS [13], such as permutation information analysis [14], [15], autocorrelation function (ACF), delayed mutual information (DMI) [16], local linear fitting in a low-dimensional subspace [8], and so on. Out of these methods, statistical methods are most widely used due to their effectiveness and robustness [17]. The primary reason for the effectiveness is the fact that the correlation between the chaotic signal $x(t)$ and its delayed version $x(t-s)$ will reach the maximum when $s=\tau$, where τ is the time delay parameter of the chaotic system [18]. An enormous amount of research effort goes into suppressing this statistical characteristic of TDS [19]–[22]. Unfortunately, it is recently discovered that there is still some security vulnerability from the perspective of dynamics. Based on the strong nonlinear inversion capability of deep learning, a TDS identification method has been proposed [23], which brings new threats to optical chaos communication. The method can identify the TDS of some security enhanced systems, even when statistical analysis loss their effectiveness.

To eliminate the weakness mentioned above, we propose a new method that one can improve the security through increasing the dimension of the chaos system and concurrently reducing the dimension of output signals. A three-dimensional (3D) EO chaos system with three coupled nonlinear feedback loops and a single-signal induced chaos synchronization method are proposed in this paper. On the other hand, chaotic synchronization is a practical issue that affects the transmission performance. Since the transmitter is specially designed to resist TDS attack, a corresponding synchronized receiver is indispensable. As a side effect, the complex structure at the receiver side could bring about the difficulty of matching multiple physical parameters. Deep learning technique has advantages in nonlinear modeling

Manuscript received December 25, 2021; accepted December 28, 2021. Date of publication December 31, 2021; date of current version January 19, 2022. This work was supported in part by the National Key Research and Development Program of China under Grant 2021YFB2900901, in part by the National Natural Science Foundation of China under Grant 62175077, in part by the Science and Technology Planning Project of Shenzhen Municipality under Grant JCYJ20200109144012410, and in part by the Hubei Key Laboratory of Intelligent Geo-Information Processing, China University of Geosciences, China under Grant KLIGIP-2019B11. *(Corresponding author: Xiaojing Gao.)*

Huaxi Huang and Zhenhua Li are with the School of Computer Science, China University of Geosciences, Wuhan 430074, China (e-mail: 965960601@qq.com; zhli@cug.edu.cn).

Xiaojing Gao is with the School of Computer Science, China University of Geosciences, Wuhan 430074, China, and also with the Hubei Key Laboratory of Intelligent Geo-Information Processing, China University of Geosciences, Wuhan 430078, China (e-mail: Gaoxj@cug.edu.cn).

Mengfan Cheng is with the Research Institute of Huazhong University of Science and Technology in Shenzhen, Shenzhen 518000, China, and also with the Next Generation Internet Access National Engineering Lab., School of Optical and Electronic Information, Huazhong University of Science and Technology, Wuhan 430074, China (e-mail: chengmf@mail.hust.edu.cn).

Digital Object Identifier 10.1109/JPHOT.2021.3139725

of chaos system [24]–[26]. Therefore, we establish the receiver in a hybrid way. Analog hardware EO link is cooperated with an artificial neural networks (ANN) in digital domain to realize the chaos synchronization. A subsystem of the chaotic transmitter is learned by the ANN. The trained ANN can reproduce the nonlinear dynamics of the subsystem at receiver for the realization of chaos synchronization. To do this work, long short-term memory neural network (LSTM-NN) is adopted. The LSTM has unique advantages of learning the long-term dependencies and effectively filtering out the noise [27]. The simulation results show that the TDS concealment and chaotic synchronization can be achieved successfully.

II. System Construction and Dynamic Characteristics

The schematic of the 3D EO chaos system is illustrated in Fig. 1. The light emitted from a continuous wave (CW) laser is injected into three paralleled EO feedback loops. In the second loop, the output of the Mach–Zehnder modulator (MZM2) is divided into two parts. One part is received and converted into an electric signal by a photodiode (PD1). After a radio-frequency amplifier (RF1), we can get an electric signal $x_1(t)$. After being delayed, the other part is received by PD3 and RF3 to generate an electric signal $x_3(t)$. Signal $x_1(t)$ and $x_3(t)$ are divided separately into two parts by electrical power splitters (ES1 and ES2). One part from signal $x_1(t)$ and one part from signal $x_3(t)$ are superimposed by ES3, then the electric mixture is used to drive MZM3 in the third loop. The other part from signal $x_1(t)$ and the other part from signal $x_3(t)$ are used as the arm working voltage of the MZM1 in the first loop. The light from MZM1 is mixed with the light from MZM3, and the optical mixture is detected by PD2 to generate an electric signal. Then the signal is amplified by RF2 to generate signal $x_2(t)$, which is used to drive MZM2.

Considering the time delay induced by the whole feedback loop, the mathematical model of the system can be written by the following equation:

$$\begin{cases} \frac{dx_1}{dt} = -x_1 - a\int_0^t x_1(s)ds + \beta_1 \cos^2(x_2 + \varphi_1) \\ \frac{dx_2}{dt} = -x_2 - a\int_0^t x_2(s)ds + \beta_2 \cos^2(x_1 - x_3 + \varphi_2) \\ \qquad + \beta_3 \cos^2(x_1 + x_3 + \varphi_3) \\ \frac{dx_3}{dt} = -x_3 - a\int_0^t x_3(s)ds + \beta_4 \cos^2(x_2(t-\tau) + \varphi_1) \end{cases} \tag{1}$$

where $x_i(t)$ is the state variable, $x_i(t-\tau)$ is the time delay feedback variable, τ is the intrinsic time delay, a is the response time of the feedback loop, β_i is the feedback strength, and φ_i is the offset phase, $i = 1, 2, 3, 4$. The dynamical characteristic of system (1) is demonstrated by numerically solving (1) based on the fourth-order Runge–Kutta method. The route to chaos is visualized in Fig. 2, where we plot the maxima of $x_2(t)$ versus the bifurcation parameter β_i, $i = 1, 2, 3, 4$. System parameters are given as $a = 5 \times 10^{-6}$, $\varphi_1 = \varphi_2 = \varphi_3 = \varphi_4 = -\pi/4$, $\beta_1 = 5$, $\beta_2 = 3.5$, $\beta_3 = 3.5$, $\beta_4 = 5$, $\tau = 20ns$. Bifurcation parameter β_i varies in the range of $0.02 \le \beta_i \le 5$ with a fixed step size of $h = 0.02$. The proposed system can enter the chaos regime with a low feedback gain for β_2, β_3 and β_4, which can reduce the difficulty of physical implementation, such as the half-wave voltage of MZM and the gain of radio-frequency amplifier.

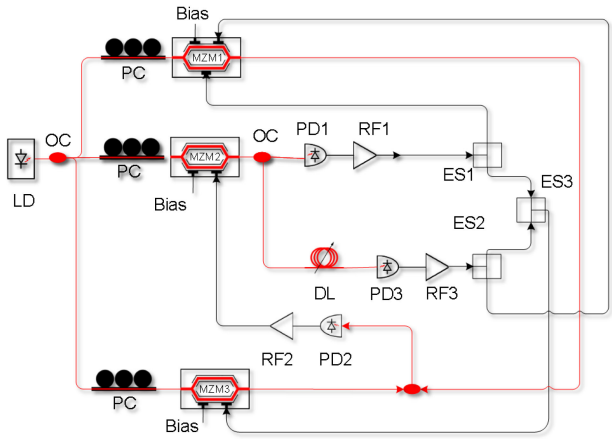

Fig. 1. Schematic diagram of system (1). LD, laser diode; MZM, Mach-Zehnder modulator; RF, radio-frequency amplifier; PD, photodiode; DL, delay line; OC, optical coupler; PC, polarization controller; ES, electrical power splitter.

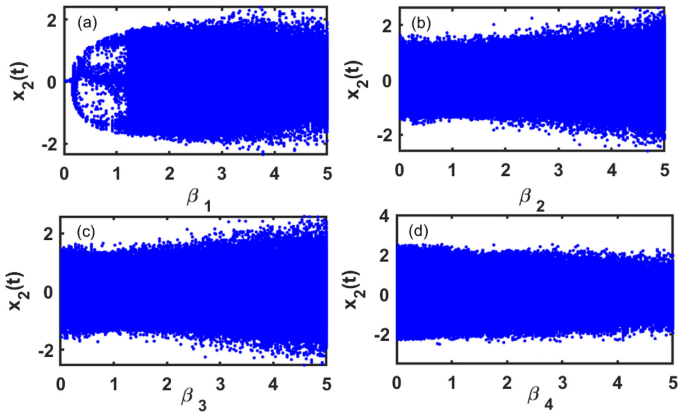

Fig. 2. The bifurcation diagram for single bifurcation parameter β_1(a), β_2(b), β_3(c), and β_4(d).

III. Synchronization Scheme and Main Numerical Results

For 3D system (1), it will be more challenging to select the multi-parameter well-matched transmitters and receivers. To overcome this problem, a NN-based single-signal symmetric induced synchronization method is proposed. The response system is theoretically designed as:

$$\begin{cases} \frac{dy_1}{dt} = -y_1 - a\int_0^t y_1(s)ds + \beta_1 \cos^2(x_2 + \varphi_1) \\ \frac{dy_2}{dt} = -y_2 - a\int_0^t y_2(s)ds + \beta_2 \cos^2(y_1 - y_3 + \varphi_2) \\ \qquad + \beta_3 \cos^2(y_1 + y_3 + \varphi_3) \\ \frac{dy_3}{dt} = -x_3 - a\int_0^t y_3(s)ds + \beta_4 \cos^2(x_2(t-\tau) + \varphi_1) \end{cases} \tag{2}$$

where $y_i(t)$ is the state variable. At the driving side (1), the output of MZM2 is divided into three parts. One part is transmitted to the response system, then chaos synchronization will be achieved, which means that system (2) is synchronized with system (1)

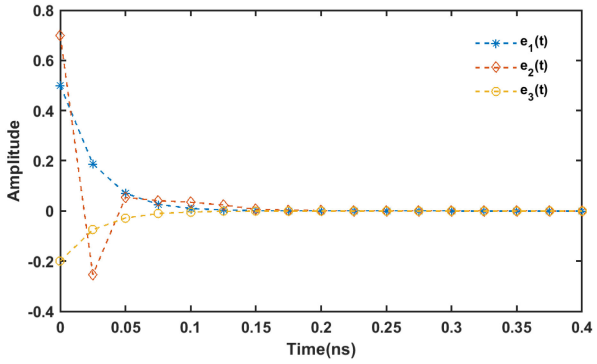

Fig. 3. Synchronization error curves of drive system (1) and response system (2).

for any initial conditions, in the sense that $\lim_{t\to\infty}\|e(t)\| = 0$, where $\|\cdot\|$ is the Euclidean norm, $e(t) = (e_1(t), e_2(t), e_3(t))$ is the error vector, $e_i = y_i - x_i$ for $i = 1, 2, 3$. The initial conditions are set as $x(0) = (0, 0.5, 1.5)$, and $y(0) = (0.5, 1.2, 1.3)$, in our simulation. Equations (1) and (2) are carried out by fourth order Runge-Kutta algorithm with an integration step of $0.625ps$. The synchronization error $e(t)$ is shown in Fig. 3, the trajectories of the drive and the response systems achieve synchronization swiftly.

For communication, at the emitter side, the message is mixed with the chaotic carrier from MZM2 in the second loop, and the light mixture is divided into three parts. One part is fed back into the 3D system which can be described as:

$$\begin{cases} \frac{dx_1}{dt} = -x_1 - a\int_0^t x_1(s)ds + \beta_1(\cos^2(x_2+\varphi_1) + m(t)) \\ \frac{dx_2}{dt} = -x_2 - a\int_0^t x_2(s)ds + \beta_2\cos^2(x_1 - x_3 + \varphi_2) \\ \qquad + \beta_3\cos^2(x_1 + x_3 + \varphi_3) \\ \frac{dx_3}{dt} = -x_3 - a\int_0^t x_3(s)ds + \beta_4(\cos^2(x_2(t-\tau) + \varphi_1) \\ \qquad + m(t-\tau)) \end{cases} \tag{3}$$

it is noteworthy that there will be an exact functional relationship between the history and future in system (1), which can be expressed as:

$$\Psi : x_1(t), x_3(t) \to x_2(t), \tag{4}$$

in the training stage, building a multi-input single-output model, we use time series $x_1(t)$ and $x_3(t)$ as the input and the desired output of an artificial neural network (ANN), then an approximate mapping function $\aleph$ to Ψ will be obtained. At the receiver side, the partial nonlinear dynamics of the chaos system is learned and replaced by an artificial neural network (ANN), as illustrated in Fig. 4. The captured light signal $s(t)$ is split into three portions $s_1(t)$, $s_2(t)$ and $s_3(t)$. Light signal $s_1(t)$ is received and converted into an electric signal by PD1. After being amplified by RF1, the response signal $y_1(t)$ is generated, i.e., $y_1(t) \approx x_1(t)$. After being delayed, light signal $s_2(t)$ is received and converted into an electric signal by PD2. After being amplified by RF2, the response signal $y_3(t)$ is generated, i.e., $y_3(t) \approx x_3(t)$. The signal $y_1(t)$ and $y_3(t)$ are converted respectively to digital signals by analogue-to-digital converters (ADC1 and ADC2) and then are put into model $\aleph$ to generate

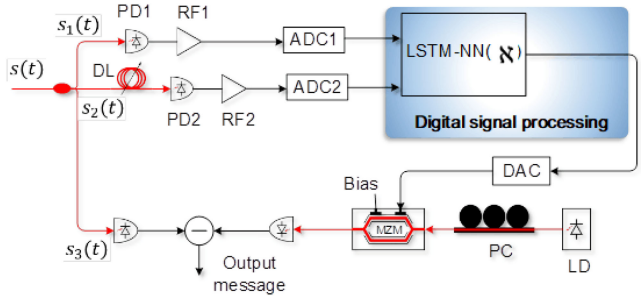

Fig. 4. Schematic diagram of single signal induced synchronization via LSTM-NN.

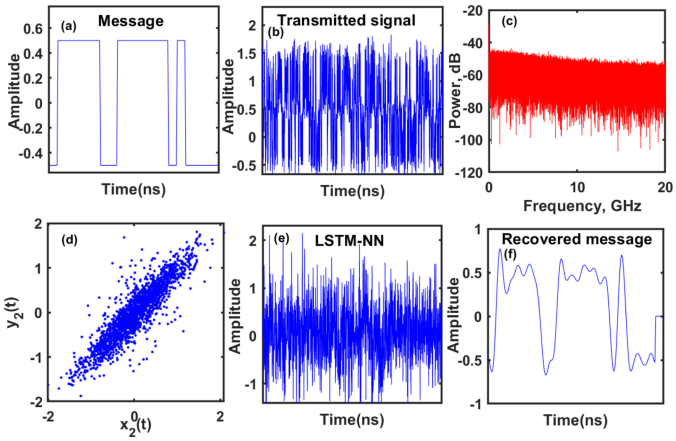

Fig. 5. Message encoding/decoding. (a) The waveform of message $m(t)$, (b) Transmitted signal and (c) corresponding spectrum, (d) chaotic synchronization plot of the chaotic time series $x_2(t)$ and $y_2(t)$, (e) chaotic time series $y_2(t)$ generated by the NN, (f) the decrypted signal at the output of low pass filter.

signal $y_2(t)$, i.e., $y_2(t) \approx x_2(t)$. Signal $y_2(t)$ is converted by DAC and then put into the MZM.

The message is decoded by subtracting the total transmitted signal $s_3(t)$ (not fed back into the receiver system) from the output of the receiver, which is known as an 'open-loop' configuration.

The corresponding receiver can be written as:

$$\begin{cases} \frac{dy_1}{dt} = -y_1 - a\int_0^t y_1(s)ds + \beta_1(\cos^2(x_2(t) + \varphi_1) + m(t)) \\ y_2 = \aleph(y_1, y_3) \\ \frac{dy_3}{dt} = -y_3 - a\int_0^t y_3(s)ds + \beta_4(\cos^2(x_2(t-\tau) + \varphi_1) \\ \qquad + m(t-\tau)) \end{cases} \tag{5}$$

according to (3) and (5), the transmission performance is demonstrated in Fig. 5. The data rate is set as 4 Gbps, and the signal-to-noise ratio (SNR) for the transmission channel is set as 15 dB. The LSTM-NN is used to model the underlying dynamical system. The modeling and forecasting are carried out by using the built-in toolkit in MATLAB2018b. The number of hidden units is set as 200. A 50 size fully connected layer and a drop layer with a drop probability of 0.5 are created. The solver 'Adam' is used to train with a mini-batch size of 20. Initial learning rate is set as 0.01. The gradient threshold is set as 1. The number of training iterations (MaxEpochs) is given as 50. The

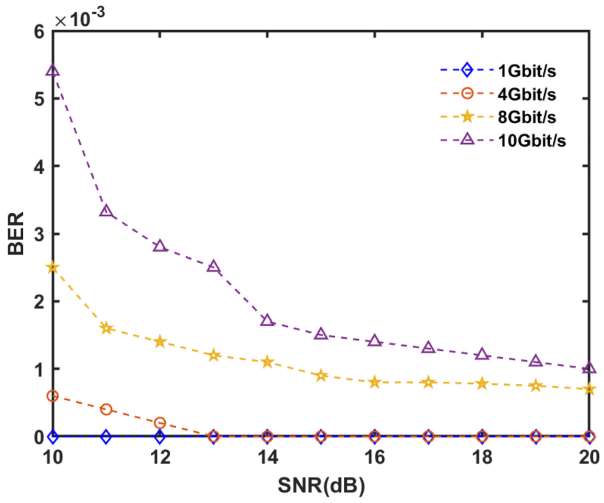

Fig. 6. BER versus SNR for different data rates.

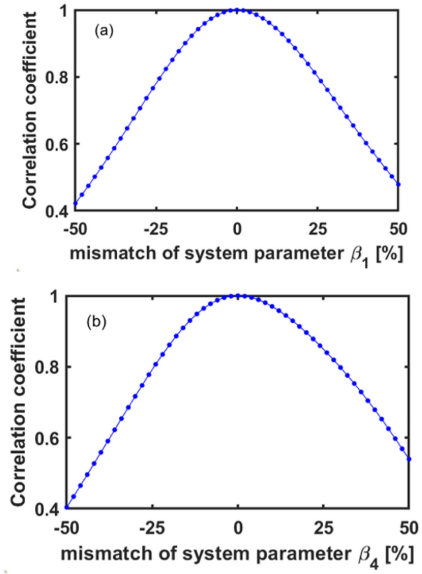

Fig. 7. Influence of system parameter β_1 (a) and β_4 (b) mismatch on the correlation coefficient.

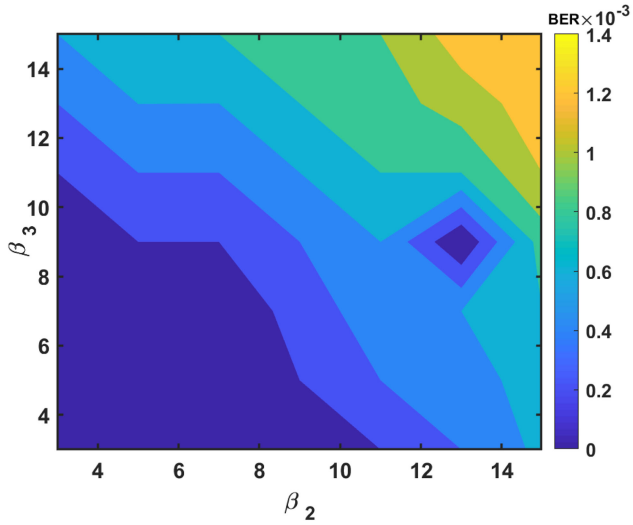

Fig. 8. The influence of the strength of nonlinearity i.e. the feedback gain β_2, β_3 on BER performance.

waveform of message $m(t)$ is plotted in Fig. 5(a). Emitter (3) generates a chaotic carrier signal with a broad power spectrum, as shown in Figs. 5(b) and (c). There are no clear signatures that can be extracted to break the security. Upon injection of the single signal from emitter into the receiver, the receiver becomes chaotic and synchronizes with the emitter, as shown in Fig. 5(d). Then the message can be reliably recovered, as illustrated in Fig. 5(f).

IV. BER Performance

The aim of this section is to study the performance of the communication system described in Figs. 1 and 4. In a real-world communication environment, the problems of system parameters mismatch and noise pollution are inevitable. Therefore, through detailed analysis, the bit error rate (BER) performance under additive white Gaussian noise channel environments with different signal to noise ratio (SNR) is studied. In Fig. 6, the BER is depicted as a function of the SNR for different data rates (1, 4, 8, 10Gbit/s). It can be observed that the BER is negatively correlated with the SNR and the data rate. When the data rate is less than 8Gbit/s, even in nonideal channel environments (e.g. SNR=10 dB), the BER performance can meet the basic requirements of communication standards (BER $< 2.5 \times 10^{-3}$). As the data rate reaches 10Gbit/s, available transmission can be maintained when SNR > 12 dB.

Moreover, the robustness against parameters (feedback gains β_1 and β_4) mismatch is discussed, which is evaluated by calculating correlation coefficient of the time series $x_2(t)$ and $y_2(t)$ when certain mismatch is intentionally introduced. Fig. 7 presents the correlation coefficient as a function of the detuning of feedback strength and time-delays. As shown in Fig. 7, when the detuning of β_1 or β_4 grows to 15%, high-quality synchronization (correlation coefficient > 0.9) can still be achieved.

We also analyse the BER performance of the proposed system under the influence of the strength of nonlinearity i.e. the feedback gain β_2, β_3. Varying β_2 and β_3 in the range of $[3, 15]$ with a fixed step size $h = 2$, we map BER in the two-dimensional (2D) plane $(\beta_2 - \beta_3)$ as shown in Fig. 8, when data rate= 4Gbit/s, SNR= 15 dB. The results show that error free transmission can be maintained if $\beta_2 < 8$ and $\beta_3 < 8$. The BER performance will decrease gradually as the feedback gain increase for $\beta_2 > 8$ or $\beta_3 > 8$. This phenomenon can be explained as follows: the nonlinearity of the system is stronger as the feedback gain increases, then the quality of chaos synchronization by using an approximate model based on NN will deteriorate, which will lead to the decrease of the BER performance. Even so, when β_2 and β_3 increase to 15 which is the upper limit of what can be achieved experimentally, available BER can be obtained (BER $< 1.4 \times 10^{-3}$).

V. Time Delay Signature Analysis

The security of the system mainly depends on the concealment of the TDS. From system (1), there is an exact underlying

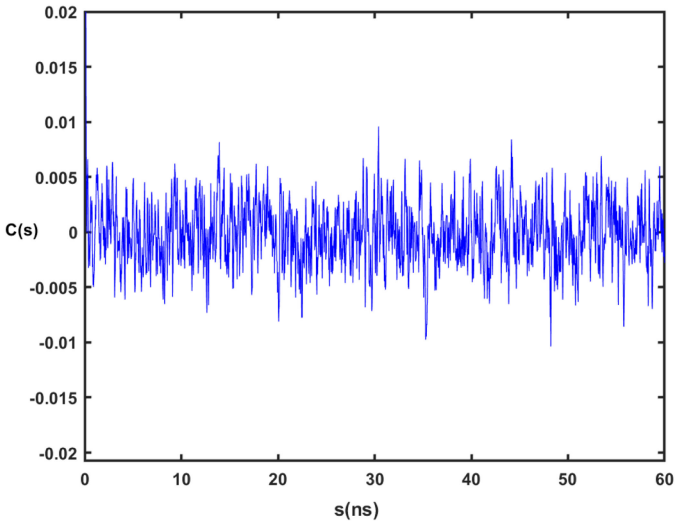

Fig. 9. Autocorrelation function with 4×10^5 data points was used.

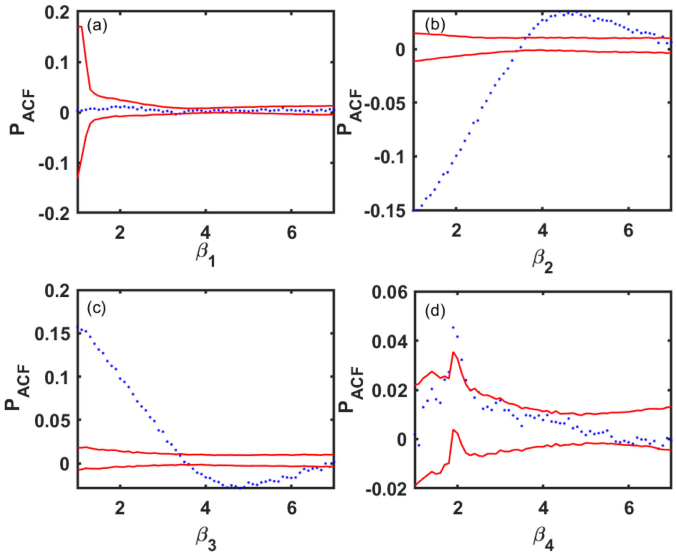

Fig. 10. Value of the peak at $s = \tau$ from the background Q_{ACF} in ACF. The red lines correspond to the background mean value and the standard deviation. (a) for β_1, (b) for β_2, (c) for β_3, and (d) for β_4.

mapping relationship between variables $x_3(t)$ and $x_2(t-\tau)$, which can be expressed as:

$$x_2(t-\tau) \to x_3(t), \tag{6}$$

to extract the TDS (i.e., τ) from the perspective of dynamics through reverse modeling, an intruder should obtain a pair of signals $(x_2(t), x_3(t)$. But in our system, just one-dimensional light signal $cos^2(x_2(t)+\varphi_1)$ from MZM2 is observable for data secure transmission. Therefore, "deficiency of data dimensionality" will cause reverse modeling attack failure. In general, statistical analysis methods including ACF and DMI are used to evaluate the confidentiality of TDS. In our communication systems (3) and (5), the time delay parameter τ is set as the encryption key whose security level is tested by using ACF in this paper. For a time series $x(t)$, ACF is defined as follows [28]:

$$C(s) = \frac{\langle [x(t) - \langle x(t) \rangle][x(t-s) - \langle x(t) \rangle] \rangle}{[x(t) - \langle x(t) \rangle]^2} \tag{7}$$

where $\langle \cdot \rangle$ stands for time average, and $x(t-s)$ is a time delayed version of $x(t)$.

As shown in Fig. 9, in the range of $0.025ns \le s \le 60ns$ with a fixed step size of $h = 0.025ns$, there are no obvious extremums at $s = 20ns$ when the encryption key $\tau = 20ns$. It is evident that an intruder cannot extract the TDS utilizing ACF by relying solely on the single-signal transmitted from system (1). In addition, the influence of the feedback strength β_i on the TDS concealment is analyzed in detail, $i = 1, 2, 3, 4$. Fig. 10 shows the size of the peak P_{ACF} at the relevant time delay $\tau = 20ns$ from the background (red lines) E_{ACF} in ACF(x_2). E_{ACF} and P_{ACF} are defined as:

$$\begin{aligned} E_{\mathrm{ACF}} &= [\underline{P}_{\mathrm{ACF}}(\beta_i), \bar{P}_{\mathrm{ACF}}(\beta_i)] \\ \underline{P}_{\mathrm{ACF}}(\beta_i) &= \mathrm{mean}\left\{\mathrm{ACF}\left(x_{\beta_i}\right)\right\} - SD\left(\mathrm{ACF}\left(x_{\beta_i}\right)\right) \\ \bar{P}_{\mathrm{ACF}}(\beta_i) &= \mathrm{mean}\left\{\mathrm{ACF}\left(x_{\beta_i}\right)\right\} + SD\left(\mathrm{ACF}\left(x_{\beta_i}\right)\right) \\ P_{\mathrm{ACF}}(\beta_i) &= \mathrm{ACF}(s = 20ns) \end{aligned} \tag{8}$$

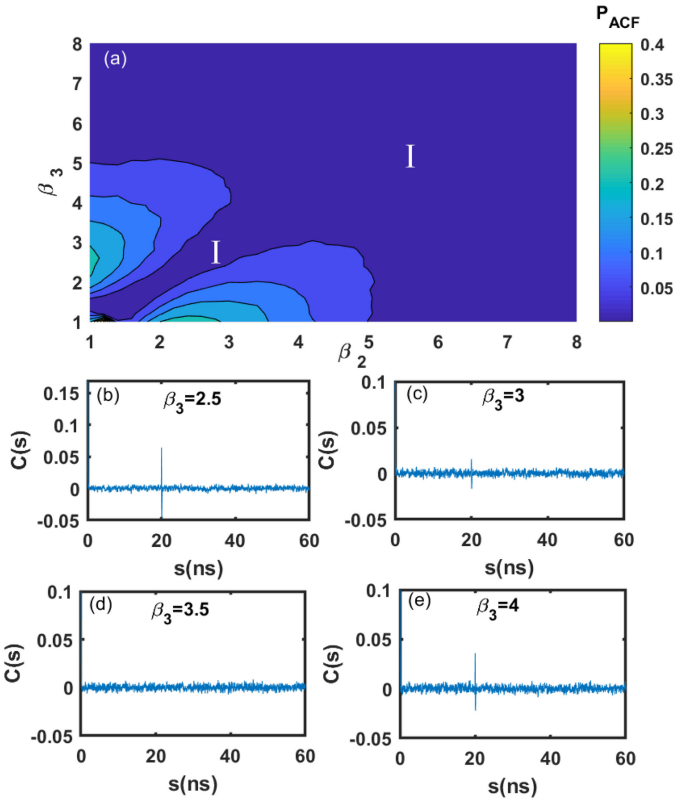

Fig. 11. (a) Influence of the feedback strengths (β_2 and β_3) on the TDS concealment, (b)–(e) The performance of TDS concealing for $\beta_3 = 2.5, 3, 3.5$ and 4 when $\beta_2 = 3.5$.

where SD is the standard deviation. Varying β_i in the range of [1,7] with a fixed step size $h = 0.1$, Fig. 10 shows the simulation results. As shown in Figs. 10(a) and (d), the peak sizes at $s = 20ns$ gradually disappear with the increase of feedback gains (β_1 and β_4). In the other words, the security of the TDS

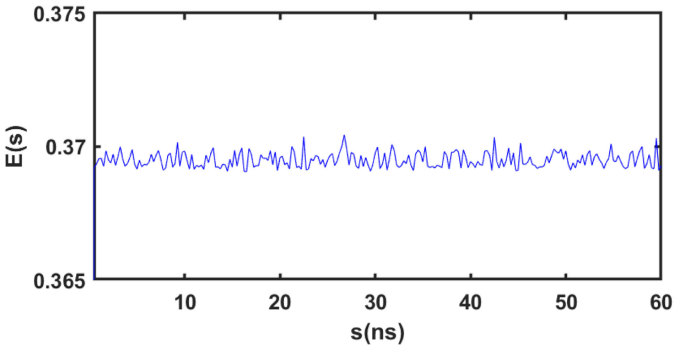

Fig. 12. The Mean Square Error (MSE) function versus s.

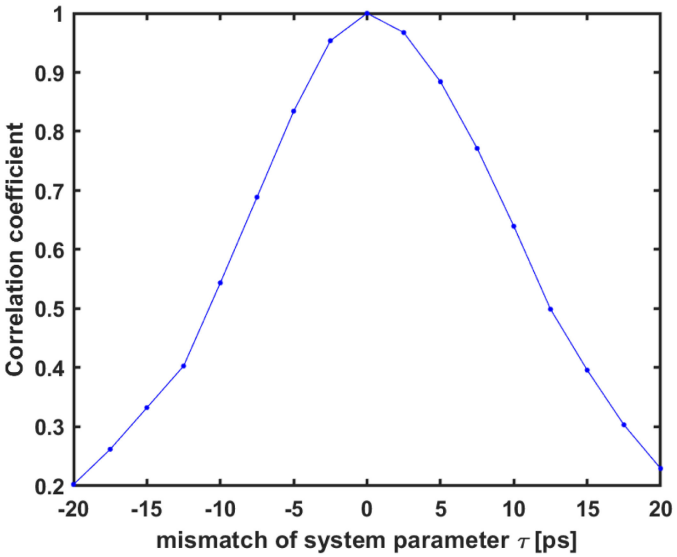

Fig. 13. Influence of system parameter τ mismatch on the correlation coefficient.

is positively correlated with the feedback parameters β_1 and β_4. However, the same conclusion is not exhibited in Figs. 10(b) and (c). For β_2 (or β_3), when the value is less than 3.5, the amplitude of the peak decreases as the parameter increases. But when the value is greater than 3.5, the peak will go beyond the background which means that TDS can be identified. For this phenomenon, we speculate that the values of system parameters β_2 and β_3 will directly affect the coupling ratio of the two feedback signals ($cos^2(x_1 - x_3 + \varphi_2)$, $cos^2(x_1 + x_3 + \varphi_3)$) in system (1), which may affect the TDS concealment.

Therefore, varying β_2 and β_3 in the range of [1,8] with a step size $h = 0.2$, we map the P_{ACF} in 2D plane $(\beta_2 - \beta_3)$ as shown in Fig. 11(a). The bule zones (noted by I) indicate successful TDS concealment of the system (1). The simulation results show that when the values of β_2 and β_3 are lower than 6.7, the interval between the two parameters will primarily affect the TDS concealment. For example, the ACF curves for $\beta_3 = 2.5, 3, 3.5, 4$ are plotted in Fig. 11(b)-(e), where the parameter β_2 is kept constant (i.e. $\beta_2 = 3.5$). It is found that the peak disappears with the decrease of the interval. Moreover, for $\beta_2, \beta_3 \geq 6.7$, there are no obvious peaks meaning that the TDS can be successfully masked.

It is worth noting that resistance to statistical analysis does not mean resistance to reverse model analysis [23]. Even if the nonlinearity of the loop transformation is increased meaning that ACF will fail, TDS can be extracted successfully by using the method proposed in [23]. Under different time delay candidate $s = \tau_j$, a neural network can be trained by using a signal intercepted from the communication channel and its time delayed version to get a model $\aleph_j$, $j = 1, \ldots$. TDS identification can be established by evaluating the prediction ability of the model $\aleph_j$. In our simulation, the prediction ability of the model $\aleph_j$ is evaluated using mean square error (MSE), which is given by (9).

$$E = \frac{1}{N}\sum_{i=1}^{N}(y_i - x_i)^2 \tag{9}$$

where $\{x_i\}$ is the expected output of a historical sequence $\{x_i\}_p^q$, $\{x_i\} = \{x_i\}_{p+s_i}^{q+s_i}$. $\{y_i\}$ is the output of model $\aleph_j$, which is the future state predicted from $\{x_i\}_p^q$. Then a MSE curve $E(s)$ can be obtained, as shown in Fig. 12. Like the statistical analysis methods, the same conclusion is exhibited. There are no obvious extremums at $s = 20ns$. The TDS $\tau = 20ns$ should be concealed successfully.

In terms of security, it is critical to ensure the sensitivity to time delay τ to prevent eavesdroppers obtaining the information. As shown in Fig. 13, even a mismatch of $20ps$ will cause the synchronization quality degrade seriously (correlation coefficient $= 0.2$). These results indicate that the communication system is very sensitive to the encryption key i.e. TDS.

VI. Conclusion

Chaotic optical communications can provide high-level physical layer security for optical secure communication. Time delayed optical chaos system has been highlighted because of its easy controllability and implementation. However, it is well known that the time delay signature (TDS, i.e., encryption key) can be inferred via statistical correlation analysis. Previous studies have focused on TDS suppression by eliminating the statistical features. Unfortunately, it is found that there is still some security vulnerability from the perspective of dynamics. On the other hand, trading off security and high-quality chaos synchronization is a challenge to be addressed. Therefore, the combining investigation on the TDS and chaos synchronization have been investigated. A new 3D EO chaotic system and a single-signal induced synchronization strategy have been designed. Moreover, in our communication system, a hybrid receiver is designed. The nonlinear model of the receiver is studied and replaced by an approximate NN model. The results show that, our method can produce the followings: first, TDS concealment caused by the deficiency of data dimensionality and multidimensional nonlinear coupling; second, high-quality chaotic synchronization can be achieved more simply via a deep-learning-based method.

REFERENCES

[1] A. Zhao, N. Jiang, S. Liu, Y. Zhang, and K. Qiu, "Physical layer encryption for WDM optical communication systems using private chaotic phase scrambling," *J. Lightw. Technol.*, vol. 39, no. 8, pp. 2288–2295, 2021.

[2] J. Ke *et al.*, "32 Gb/s chaotic optical communications by deep-learning-based chaos synchronization," *Opt. Lett.*, vol. 44, no. 23, pp. 5776–5779, 2019.

[3] M. Zhang and Y. Wang, "Review on chaotic lasers and measurement applications," *J. Lightw. Technol.*, vol. 39, no. 12, pp. 3711–3723, 2021.

[4] A. Zhao, N. Jiang, S. Liu, Y. Zhang, and K. Qiu, "Generation of synchronized wideband complex signals and its application in secure optical communication," *Opt. Exp.*, vol. 28, no. 16, pp. 23 363–23373, 2020.

[5] L. Wang *et al.*, "Scheme of coherent optical chaos communication," *Opt. Lett.*, vol. 45, no. 17, pp. 4762–4765, 2020.

[6] L. Jiang *et al.*, "Trading off security and practicability to explore high-speed and long-haul chaotic optical communication," *Opt. Exp.*, vol. 29, no. 8, pp. 12750–12762, 2021.

[7] A. Argyris *et al.*, "Chaos-based communications at high bit rates using commercial fibre-optic links," *Nature*, vol. 438, no. 7066, pp. 343–346, 2005.

[8] R. Hegger, M. J. Bünner, H. Kantz, and A. Giaquinta, "Identifying and modeling delay feedback systems," *Phys. Rev. Lett.*, vol. 81, no. 3, pp. 558–561, Jul. 1998.

[9] J. Bai, H. Wang, and Y. Ji, "Time-delay signature concealing electro-optic chaotic system with multiply feedback nonlinear loops," *Opt. Exp.*, vol. 29, no. 2, pp. 706–718, 2021.

[10] J. Chen, C. Li, X. Mu, L. Li, and Y. Duan, "Time-delay signature suppression of polarization-resolved wideband chaos in VCSELs with dual-path chaotic optical injections," *Appl. Opt.*, vol. 59, no. 24, pp. 7217–7224, 2020.

[11] R. Zhang, P. Zhou, Y. Yang, Q. Fang, P. Mu, and N. Li, "Enhancing time-delay suppression in a semiconductor laser with chaotic optical injection via parameter mismatch," *Opt. Exp.*, vol. 28, no. 5, pp. 7197–7206, 2020.

[12] D. Chen, Q. Li, and Q. Bao, "Bidirectional communication with time-delay concealment in a system combining all-optical intensity and electrooptical phase chaos," *Opt. Commun.*, vol. 465, 2020, Art. no. 124962.

[13] Y. Chen *et al.*, "Machine learning approach to unveil time delay signature of electro-optical chaotic system with strong nonlinearity," in*Proc. Asia Commun. Photon. Conf. (ACPC), OSA Tech. Dig. (Optical Soc. Amer., 2019)*, 2019, pp. T1H.3.

[14] L. Zunino, M. C. Soriano, I. Fischer, O. A. Rosso, and C. R. Mirasso, "Permutation-information-theory approach to unveil delay dynamics from time-series analysis," *Phys. Rev. E*, vol. 82, no. 4, 2010, Art. no. 046212.

[15] M. C. Soriano, L. Zunino, O. A. Rosso, I. Fischer, and C. R. Mirasso, "Time scales of a chaotic semiconductor laser with optical feedback under the lens of a permutation information analysis," *IEEE J. Quantum Electron.*, vol. 47, no. 2, pp. 252–261, Feb. 2011.

[16] D. Rontani, A. Locquet, M. Sciamanna, D. S. Citrin, and S. Ortin, "Time-delay identification in a chaotic semiconductor laser with optical feedback: A dynamical point of view," *IEEE J. Quantum Electron.*, vol. 45, no. 7, pp. 879–1891, Jul. 2009.

[17] A. Elsonbaty, S. F. Hegazy, and S. S. Obayya, "Simultaneous suppression of time-delay signature in intensity and phase of dual-channel chaos communication," *IEEE J. Quantum Electron.*, vol. 51, no. 9, pp. 1–9, Sep. 2015.

[18] S. Banerjee, *Chaos Synchronization and Cryptography for Secure Communications: Applications for Encryption: Applications for Encryption*. USA IGI global, 2011.

[19] A. Zhao, N. Jiang, S. Liu, C. Xue, and K. Qiu, "Wideband time delay signature-suppressed chaos generation using self-phase-modulated feedback semiconductor laser cascaded with dispersive component," *J. Lightw. Technol.*, vol. 37, no. 19, pp. 5132–5139, 2019.

[20] P. Mu, P. He, and N. Li, "Simultaneous chaos time-delay signature cancellation and bandwidth enhancement in cascade-coupled semiconductor ring lasers," *IEEE Access*, vol. 7, pp. 11041–11048, 2019.

[21] S. Cui and J. Zhang, "Chaotic secure communication based on single feedback phase modulation and channel transmission," *IEEE Photon. J.*, vol. 11, no. 5, Oct. 2019, Art. no. 7905208.

[22] J. Zhang and S. Cui, "Enhanced bidirection secure communication based on digital key and chaotic random optical feedback," *IEEE Photon. J.*, vol. 10, no. 6, Dec. 2018, Art. no. 7908308.

[23] X. Gao *et al.*, "Time delay estimation from the time series for optical chaos systems using deep learning," *Opt. Exp.*, vol. 29, no. 5, pp. 7904–7915, 2021.

[24] Q. Cai, Y. Guo, P. Li, A. Bogris, and Y. Wang, "Modulation format identification in fiber communications using a single dynamical node based artificial neural network," *Photon. Res.*, vol. 9, no. 1, pp. B1–B8, Jan. 2020.

[25] D. Zhong, H. Yang, J. Xi, N. Zeng, Z. Xu, and F. Deng, "Predictive learning of multi-channel isochronal chaotic synchronization by utilizing parallel optical reservoir computers based on three laterally coupled semiconductor lasers with delay-time feedback," *Opt. Exp.*, vol. 29, no. 4, pp. 5279–5294, 2021.

[26] Z. Yang, J. Ke, W. Hu, and L. Yi, "Effect of ADC parameters on neural network based chaotic optical communication," *Opt. Lett.*, vol. 46, no. 1, pp. 90–93, 2021.

[27] M. Sangiorgio and F. Dercole Yeo, "Robustness of lstm neural networks for multi-step forecasting of chaotic time series," *Chaos, Solitons & Fractals*, vol. 139, 2020, Art. no. 110045.

[28] Y. Tang, Q. Li, W. Dong, M. Hu, and R. Zeng, "Optical chaotic communication using correlation demodulation between two synchronized chaos lasers," *Opt. Commun.*, vol. 498, 2021, Art. no. 127232.